RSC Advances

PAPER

View Article Online
View Journal | View Issue

Cite this: *RSC Adv.*, 2024, **14**, 31730

Preparation and demulsification performance of magnetic demulsifier Fe_3N@F

Chao Liu, [ab] Xinlei Jia,*[c] Yonghui Wang,[c] Yanjuan Liu,[b] Weining Qin[b] and Lixin Wei[ab]

Received 1st August 2024
Accepted 1st October 2024

DOI: 10.1039/d4ra05569a

rsc.li/rsc-advances

Given the suboptimal emulsification performance and the potential for secondary pollution posed by existing demulsifiers, a facile and highly efficient fluorinated magnetic demulsifier (Fe_3N@F) was synthesized *via* a one-step approach using fluorinated polyether and iron nitride as raw materials.The morphology and structure of the demulsifier were characterized using Fourier transform infrared spectroscopy (FTIR), scanning electron microscopy (SEM), thermogravimetric analysis (TGA), and X-ray photoelectron spectroscopy (XPS). The results confirm a successful fluoropolyether coating on the surface of iron nitride. The demulsifying and dehydrating properties were assessed through demulsifying and dehydrating experiments, and the influence of demulsifier addition and demulsifying temperature on the demulsification performance was investigated. Additionally, the demulsification mechanism was analyzed by the microscopic demulsification process. The results indicated that under the condition of the optimum demulsification temperature of 45 °C and the optimum demulsifier dosage of 150 mg L^{-1}, the water removal (%) of the magnetic demulsifier containing fluorine (Fe_3N@F) was the highest, and could reach 89.4%. Fe_3N@F exhibited excellent magnetic response, the demulsifying rate could reach above 70% after recycling and reusing it 6 times. The application of iron nitride in demulsification presents a novel thought for the advancement of magnetic demulsifiers.

1. Introduction

During the process of crude oil extraction, production, and refining, a significant amount of crude oil emulsions is inevitably generated due to shearing, heating, and other factors. Additionally, the high content of oil, heavy metal ions, salts, solid suspended particles, and high molecular polymers in Chinese crude oil leads to interactions that result in cross-linking and emulsification processes. These interactions contribute to the enhanced stability of crude oil emulsions and the formation of complex emulsion systems such as W/O, O/W, and multiple emulsions.[1–3] Inadequate handling may result in environmental pollution, adverse effects on human health, and corresponding resource wastage. The usage of chemical reagents for demulsification represents the prevailing method due to its economic efficiency and efficacy. In recent years, driven by production and operational demands, demulsification systems have matured. However, chemical demulsifiers still exhibit poor universality and present potential ecological hazards, as well as issues related to complex processes and significant expenses. Therefore, it is imperative to develop an economical, efficient, and environmentally friendly new type of demulsifier.[4–6] The polyether demulsifiers are currently the most extensively researched and utilized demulsifiers, and their unique design versatility allows researchers to synthesize a variety of polyether demulsifiers tailored to the characteristics of different crude oil compositions.[7,8] Jian *et al.*[9] investigated the impact of Hydrophobically modified polyacrylamide (HMPAM) containing cationic, anionic, and nonionic hydrophobic monomers on the demulsification efficiency of D1 for W/O emulsion of heavy oil. The nature and length of the hydrophobic monomer in HMPAM have implications for the ultimate water separation by D1. Jingjing *et al.*[10] proposed a nano-modification strategy utilizing epoxy-functionalized magnetic nanoparticles and carboxylated poly(epoxypropyl)–poly(-ethyleneoxide) block copolymer to fabricate highly efficient demulsifiers. The outstanding demulsifying capability of the nanomodified carboxylated polyether was confirmed through bottle testing and molecular dynamics simulation analysis. Zhang *et al.*[11] synthesized a tri-blocked polyether demulsifier by crosslinking bisphenol A phenolamine resin (BPA) with a tri-blocked polyether, achieving a 92.5% water removal efficiency at 50 °C, with a dosage of 75 mg L^{-1} and pH of 7.6 over a period of 90 minutes. The fluorinated surfactants demonstrate exceptional surface activity, characterized by heightened thermal stability, hydrophobicity, and lipophobicity, as well as superior wetting and flocculation properties. They effectively modulate the oil–water interface to achieve emulsification and water

[a]*Heilongjiang Provincial Key Laboratory of Oilfield Applied Chemistry and Technology, Daqing Normal University, Daqing, 163712, China*

[b]*Key Laboratory of Enhanced Oil Recovery, Northeast Petroleum University, Ministry of Education, Daqing, 163318, China*

[c]*College of Chemical Engineering and Safety, Shandong University of Aeronautics, Binzhou, 256603, China. E-mail: 18434362466@163.com*

removal.[12,13] Wei *et al.*[14] synthesized self-*p*-trifluoromethylphenol using phenolamine resin as an initiator, and then, by means of block copolymerization with epoxyethane and epoxypropane as raw materials, they prepared fluorinated polyether demulsifier, under the condition of 60 °C and 100 mg L^{-1} addition, the demulsification rate of FB4 for Liaohe oilfield could reach 90.33% within 2 hours. Zhang *et al.*[15] used phenolamine resin as an initiator and used toluene diisocyanate (TDI) to crosslink the block copolymer polyether to synthesize a networked fluorinated polyether demulsifier. They obtained the optimal demulsification conditions, with the demulsification temperature set at 60 °C and the demulsifier dosage at 50 mg L^{-1}, the RBF4 demulsifier achieved a drainage rate of 95.64%. Xiaoheng *et al.*[16] used molecular dynamics simulation software to select 24 demulsifiers and determined the ability of demulsifier molecules to reduce total energy. They studied the interface destabilization caused by the collision of fluorinated polyether demulsifiers and found that the carbon–fluorine chain has positive surface activity and stability. In our preliminary research, we successfully incorporated fluorine into polyether demulsifiers, resulting in the synthesis of extremely effective fluorinated polyether demulsifiers. Nevertheless, the challenge remains in the recyclability of these demulsifiers.

In line with the principles of sustainable and environmentally friendly practices, magnetic demulsifiers have been developed. The rapid magnetic response and recyclability of magnetic nanoparticles have garnered significant attention, as they can be retrieved from oil–water emulsions using an external magnetic field, thereby enabling cost-effective recycling. Simultaneously, this approach addresses the challenges associated with traditional chemical demulsifiers that are difficult to separate and pose environmental risks.[17,18] Liu *et al.*[19] utilized the excellent adsorption properties of carbon materials to prepare a novel magnetic nanofoam demulsifier. When the addition amount was 800 mg L^{-1}, the demulsification temperature was 65 °C, and the pH value was 6, the demulsification rate of Fe_3O_4@C–F could reach 91.68% within 90 min. Feng *et al.*[20] used three commercially available polyether demulsifiers (AE1910, SP169, and AR321) and mussel-inspired poly(dopamine) as an adhesive to anchor them to Fe_3O_4 nanoparticles to prepare a novel magnetic demulsifier. The three nanoparticles all have amphiphilic properties and improved interfacial activity, and have productive demulsification rates for crude oil emulsions, reaching 98.00%, 91.63%, and 94.33% respectively. Hamed Sadighian *et al.*[21] have developed a novel, environmentally friendly, profoundly efficient, and recyclable nanomagnetic compound based on imidazole-modified cyclodextrin. This compound can achieve a 92% emulsification rate within 24 hours when the defoamer addition is at 5000 ppm for W/O emulsions. Enhanced magnetic properties have been observed in ferric nitride compared to Fe_3O_4, along with its superior attributes of elevated temperature resistance, corrosion resistance, and oxidation resistance.[22–24] Leveraging the exceptional properties of iron nitride, this study involved the surface loading of fluorinated polyether onto iron nitride material to fabricate a magnetic demulsifier Fe_3N@F. The structure and performance of the demulsifier were characterized, followed by an evaluation experiment on its demulsification efficiency using crude oil emulsion as the research subject. The preparation of this demulsifier is straightforward and yields a profoundly efficient demulsifying agent, offering a novel approach for the development of magnetic demulsifiers.

2. Experiment

2.1 Materials

Ferric nitride, Guoyao Group Chemical Reagents Co., Ltd. Anhydrous ethanol, Tianjin Tianli Chemical Reagents Co., Ltd, *n*-hexane, Tianjin Kaitong Chemical Reagents Co., Ltd. Nitrogen, Changchun Xinguang Gas Co., Ltd; petroleum ether, State Pharmaceutical Group Chemical Reagents Co., Ltd; diesel, Sinopec Gas Station; fluorinated polyether, laboratory-made; dehydrated crude oil, Daqing Oilfield, the density of this dehydrated crude oil at 25 °C is 0.847 kg m^{-3}, the viscosity at 50 °C is 35.7 mPa s, and the total water content is 0.5%. The reagents used in this laboratory are of analytical grade and are used without further purification.

2.2 Preparation of Fe_3N@F

As illustrated in Fig. 1, the Fe_3N@F demulsifier was synthesized by solvent-thermal one-step method. Add 0.2 g of ferric nitride and 0.6 g of fluorinated polyether to a beaker containing 30 mL of anhydrous ethanol. Stir the materials in the beaker evenly with a glass rod, disperse them using ultrasonic treatment for 30 minutes. Transfer the material from the beaker into a ceramic crucible, place it into a tubular electric furnace, and remove the air in the furnace by injecting nitrogen. Increase the temperature to 180 °C at a rate of 5 °C min^{-1}, carry out the reaction at high temperature for 6 hours. At the end of the reaction, remove the reactants and separate the products using magnets. Cleanse the products by adding a mixture of ethanol and *n*-hexane (1 : 1 volume ratio) two to three times. Finally, dry the product at 60 °C for 12 hours to collect it. The product

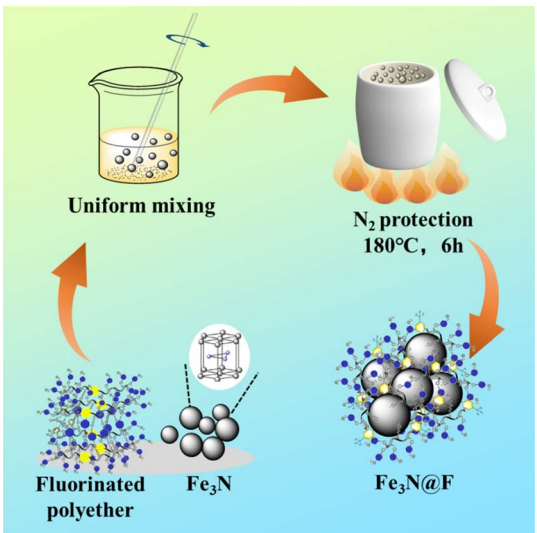

Fig. 1 Synthesis route of Fe_3N@F.

obtained from this preparation process is denoted as Fe_3N@F1. In subsequent experiments, three other Fe_3N@F magnetic demulsifiers (Fe_3N@F2, Fe_3N@F3, and Fe_3N@F4) were prepared using ferric nitride and fluorinated polyether at ratios of 1 : 5, 1 : 7, and 1 : 8 respectively.

2.3 Characterization of the structure and performance of Fe_3N@F

2.3.1 Scanning electron microscope (SEM). The structure and morphology of Fe_3N@F magnetic demulsifiers were characterized using scanning electron microscopy, yielding images at various magnifications.

2.3.2 X-ray photoelectron spectroscopy (XPS). The surface elements of Fe_3N and Fe_3N@F magnetic demulsifying agents were analyzed using X-ray photoelectron spectroscopy (XPS). The full spectrum was examined at a lower scanning resolution, while the single element analysis was performed at a higher resolution. The test results underwent peak separation fitting, and the valence of elements and chemical bond composition were analyzed.

2.3.3 Infrared spectroscopy analysis (FTIR). The IR spectra of Fe_3N@F were analyzed using Fourier transform infrared (FTIR) spectroscopy. The samples were ground with KBr in a mortar at a ratio of 1 : 100, and the spectra were scanned 32 times across the wavelength range of 400–4000 cm^{-1}.

2.3.4 Thermogravimetric analysis (TGA). Thermal analysis of Fe_3N, fluorinated polyether and Fe_3N@F was performed using a TGA/DSC1 thermal analyzer, with the samples being heated from 30 °C to 800 °C at a rate of 10 °C min^{-1} under nitrogen protection.

2.3.5 Interfacial activity test. Add 5 mL of diesel and 5 mL of distilled water to the sample bottle, followed by the separate addition of 0.01 g of Fe_3N and Fe_3N@F. Manually shake the sample bottle up and down 200 times vigorously before allowing it to settle,[25–27] then observe the distribution of the sample in the oil–water emulsion.

2.3.6 Dynamic interfacial tension test. The capability of Fe_3N@F to reduce interfacial tension was assessed using an optical contact angle goniometer. Subsequently, 200 mg L^{-1} of Fe_3N@F demulsifier was introduced into the prepared crude oil emulsion at room temperature, with the rotational speed of the suspended interfacial tension meter set to 5000 rpm.

2.3.7 Wetting test. Using an optical contact angle measuring instrument, the wetting properties of different samples were evaluated by measuring the three-phase contact angle of Fe_3N and Fe_3N@F through the pendant drop method. Before the test, the sample powder was compressed into a smooth thin sheet, and then a drop of water was dropped on the thin sheet. The change process of the water drop was recorded, and the contact angle was obtained by analyzing the shape of the water drop.

2.3.8 Magnetic analysis (VSM). The magnetic properties of Fe_3N and Fe_3N@F magnetic materials were characterized using an MPMSXL-5 vibrating sample magnetometer.

2.4 Emulsion preparation of crude oil

The presence of solid particles and other impurities in crude oil can significantly impact the determination of interfacial potential. Crude oil from a specific block in the Daqing Oilfield underwent treatment and dehydration. To ensure standardized experimental conditions, an artificially prepared emulsified crude oil was used for demulsification in the laboratory. 140 mL of dehydrated crude oil and 60 mL of distilled water were heated to 60 °C in a constant temperature water bath. Subsequently, the preheated crude oil was placed in a motorized stirrer, with distilled water added in three equal portions, each time being stirred at 3000 rpm for 60 min to achieve thorough mixing. An artificial crude oil emulsion with a water content of 30% was then created and poured into a clean beaker, left at room temperature for 24 h without any separation between the oil and water.

2.5 Evaluation of emulsifying performance

According to the SY/T 5281-2000 "Performance Test Method for Demulsifier for Crude Oil (Bottle Test Method)", the demulsification performance of various samples was assessed. Initially, 20 mL of crude oil emulsion was introduced into the sample bottle, followed by the addition of different samples. The sample bottle underwent vigorous shaking 200 times to ensure uniform dispersion of the demulsifier sample within the emulsion. Subsequently, observation and recording of demulsification effects were conducted after allowing time for settling. Moisture content determination utilized coulometry method with output configured as ratio between water volume in liquid and test liquid volume. Following completion of demulsification, one milliliter of oil phase from the emulsion was transferred to an electrolytically balanced Karl Fischer micro-water content analyzer. Upon re-establishment of electrolytic balance, automatic computation based on electricity consumption yielded water content measurement displayed on screen.

2.6 Enhanced assessment of recycling performance

The Fe_3N@F magnetic demulsifier was chosen as the subject for the recovery experiment. Following the initial demulsification test, the Fe_3N@F was retrieved using an external magnetic field, then purified with petroleum ether and dried in a vacuum oven. The desiccated Fe_3N@F demulsifier was subsequently employed in a new round of demulsification testing to assess its recycling performance.

3. Results and discussion

3.1 Characterization

3.1.1 The surface morphology of Fe_3N@F. The SEM images of nitrogen-doped iron and partial Fe_3N@F magnetic demulsifier are presented in Fig. 2. From Fig. 2(a), it is evident that the Fe_3N@F1 monomers exhibit a nearly spherical morphology with varying sizes, and are dispersed in a relatively non-uniform arrangement. In Fig. 2(b), the SEM image of Fe_3N@F2 reveals a composite material with a stochastic structure, where nitrogen-doped iron monomers are interconnected and tightly

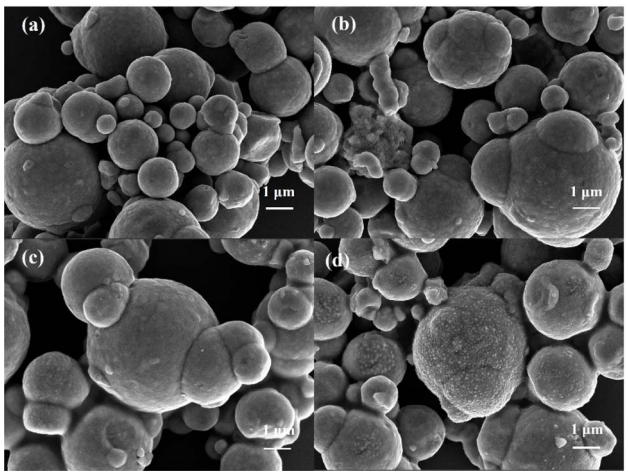

Fig. 2 SEM image of Fe_3N@F ((a) Fe_3N@F1; (b) Fe_3N@F2; (c) Fe_3N@F3; (d) Fe_3N@F4).

adhered to each other. As depicted in Fig. 2(c) for Fe_3N@F3, an increase in polyether content results in minimal presence of individual spherical particles, as connected micelles coalesce into larger vesicle-like structures. Furthermore, the SEM image of Fe_3N@F4 (Fig. 2(d)) displays a mulberry-like appearance, indicating that the fluorinated polyether not only aggregates the Fe_3N monomers but also partially attaches to their surfaces. These observations from the SEM images suggest successful integration between the Fe_3N monomers and fluorinated polyether within the composite materials.

3.1.2 X-ray photoelectron spectroscopy (XPS). Fig. 3 presents the XPS spectra of Fe_3N and Fe_3N@F. The comprehensive XPS spectrum in Fig. 3(a) demonstrates the presence of Fe, O, N, and C elements in the composite material, along with the detection of F element. The signals for Fe, F, O, N, and C elements are observed at approximately 720.19 eV, 682.01 eV, 528.19 eV, 400.43 eV, and 283.42 eV respectively. In Fig. 3(b), the N 1s spectrum is resolved into four peaks representing oxidized N (403.62 eV), graphitic N (401.31 eV), Fe–N (400.3 eV), and pyridinic-N (398.6e V). Analysis of the Fe 2p XPS spectrum in Fig. 3(c) reveals that it comprises two valence states: Fe^{2+} (7249 eV and 7106 eV) and Fe^{3+} (7332 eV and 7122e V), corresponding to the energy levels of Fe $2p_{1/2}$ and Fe $2p_{3/2}$ respectively. Additionally, two satellite peaks are also present. The XPS spectral results collectively support the successful grafting of fluorinated polyether onto nitrogen–iron.

3.1.3 FT-IR. The infrared spectra in Fig. 4 depict the fluoroether, Fe_3N@F1, and Fe_3N@F3. The peaks at 2968 cm^{-1} and 2873 cm^{-1} correspond to the asymmetric and symmetric stretching vibrations of $-CH_3$, respectively. At 1114 cm^{-1} and 932 cm^{-1}, there are corresponding asymmetric and symmetric stretching vibrations of C–O–C. The absorption peak at 1214 cm^{-1} corresponds to the C–F bond, while the absorption peak at 1008 cm^{-1} corresponds to the α-carbon of the side chain in the ether bond; this feature is absent in Fe_3N@F1 and Fe_3N@F3. Furthermore, a distinct Fe–N peak appears around 2913 cm^{-1} on the left side of the spectrum for both Fe_3N@F1 and Fe_3N@F3, providing evidence that successful grafting of fluoroether onto Fe_3N has occurred.

3.1.4 Thermogravimetric analysis (TGA). Fig. 5 illustrates the TGA profiles of Fe_3N, fluorinated polyether, and Fe_3N@F. Below 200 °C, a slight weight loss is ascribed to the evaporation of physically adsorbed water. The second stage of decomposition for fluorinated polyether commences at 315 °C, leading to

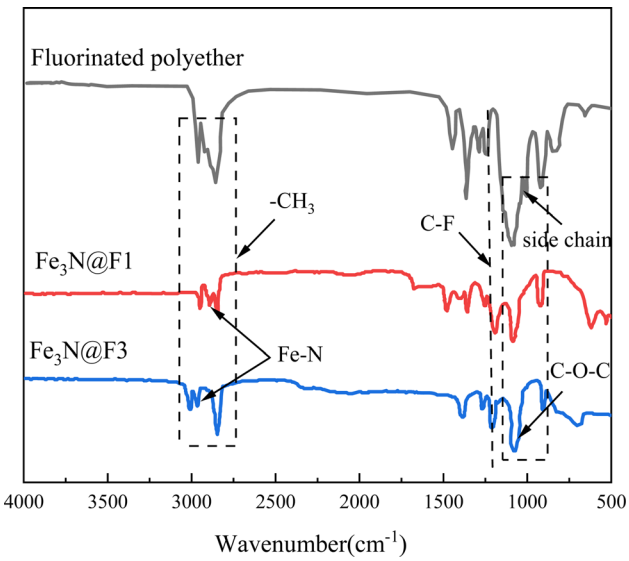

Fig. 4 FTIR spectra of fluoroether and Fe_3N@F.

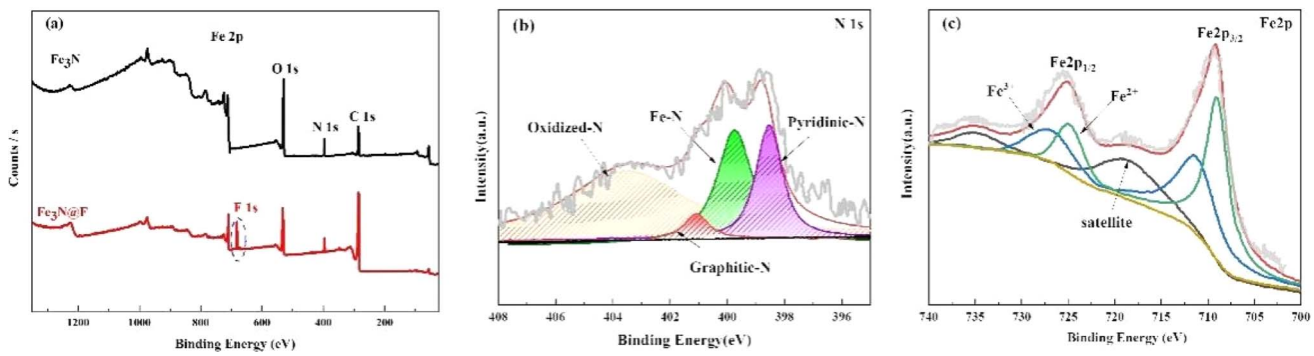

Fig. 3 X-ray photoelectron spectroscopy (XPS) spectra of (a) full spectrum of composite materials; (b) Fe_3N and (c) Fe_3N@F.

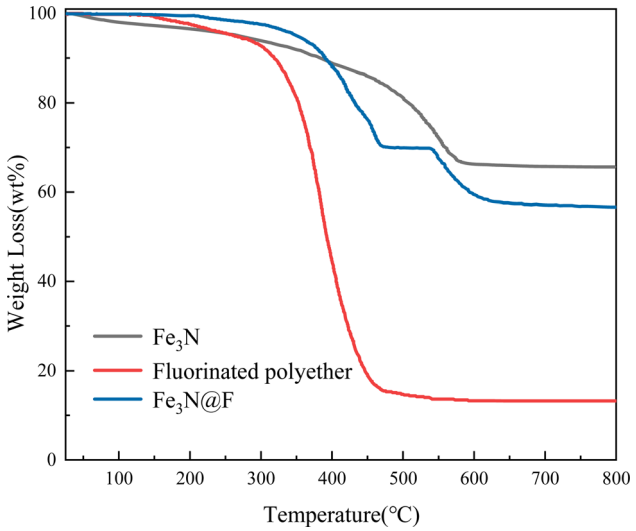

Fig. 5 TGA curves of Fe_3N, fluorinated polyether, and Fe_3N@F.

a significant weight reduction. Overall, the sample undergoes an 84% decrease in weight with complete decomposition of fluorinated polyether occurring at 480 °C, resulting in the formation of char product. Between 320 °C and 475 °C, there is a total weight loss of 27.9%, primarily due to the degradation of organic compound fluorinated polyether groups. Subsequently, between 538 °C and 633 °C, further reduction in weight occurs mainly due to the decomposition of Fe_3N. Notably, the decomposition temperature for Fe_3N@F is significantly higher than that for fluorinated polyether which provides additional evidence supporting successful grafting of nitride iron material onto the fluorinated polyether.

3.1.5 Interfacial activity. Fig. 6 illustrates the interfacial activity of magnetic demulsifiers, as well as the distribution of Fe_3N and Fe_3N@F demulsifiers within the oil–water two-phase system and at the oil–water interface. Upon observing Fig. 6(a), it is evident that prior to mixing, diesel and water are immiscible, resulting in a relatively clear oil–water interface. Subsequently, after separately adding Fe_3N and Fe_3N@F and vigorously shaking to achieve uniform mixing, as depicted in Fig. 6(b) after standing for 20 minutes, most of the ferric nitride dissolves into the oil due to its hydrophobic nature, leading to turbidity; additionally, some agglomerated particles enter the water phase while Fe_3N@F primarily localizes at the oil–water interface. Following a 24 hours period of standing, shown in Fig. 6(c), all three groups exhibit an oil–water interface state similar to their initial condition; however, there is an increased depth of emulsification which remains stable. In comparison with ferric nitride, it can be concluded that Fe_3N@F demulsifier demonstrates superior hydrophilic–lipophilic balance along with effective interfacial activity that facilitates oil–water separation.

3.1.6 The dynamic interfacial tension (IFT). The dynamic interfacial tension of various materials was measured using a suspended interfacial tension meter, as depicted in Fig. 7. In Fig. 7(a), the dynamic surface tension of perfluorinated polyether and Fe_3N@F at a concentration of 150 mg L^{-1} is presented. Both materials exhibit significant capability in reducing oil–water interfacial tension, with perfluorinated polyether demonstrating the highest efficacy by lowering the emulsion's interfacial tension from 44.8 mN m^{-1} to 14.5 mN m^{-1}. Additionally, the dynamic interfacial tension of the emulsion containing Fe_3N@F decreases from 44.4 mN m^{-1} to 20.1 mN m^{-1} with increasing Fe_3N@F concentration, as illustrated in Fig. 7(b). Notably, when the concentration of Fe_3N@F reaches 150 mg L^{-1}, the dynamic interfacial tension of the emulsion reaches its minimum value at 19.4 mN m^{-1}, indicating favorable interfacial properties.

3.1.7 Wettability. The surface wettability of Fe_3N and Fe_3N@F composite demulsifiers was assessed using the three-phase contact angle method to evaluate their hydrophilic and oleophobic properties, as depicted in Fig. 8. In Fig. 8(a), the contact angle of Fe_3N is measured at 95.6°, indicating its insolubility in water and hydrophobic nature. Meanwhile, Fig. 8(b) illustrates that the contact angle of Fe_3N@F is approximately 89.5°, closely approaching 90°, aligning with the performance criteria for demulsifying materials. Fluorinated polyether comprises hydrophilic ethylene oxide (EO) segments and hydrophobic propylene oxide (PO), while fluorinated surfactants within it exhibit amphoteric characteristics. Research has demonstrated that demulsifiers can be simultaneously wetted by oil and water; upon reaching the oil–water interface, the hydrophilic end of Fe_3N@F enters the aqueous phase while its hydrophobic segment permeates into the oil phase. Following combination with nitride iron, fluorinated polyether achieves a favorable balance between hydrophilicity and lipophilicity, enabling effective demulsification by Fe_3N@F to achieve two-phase separation.

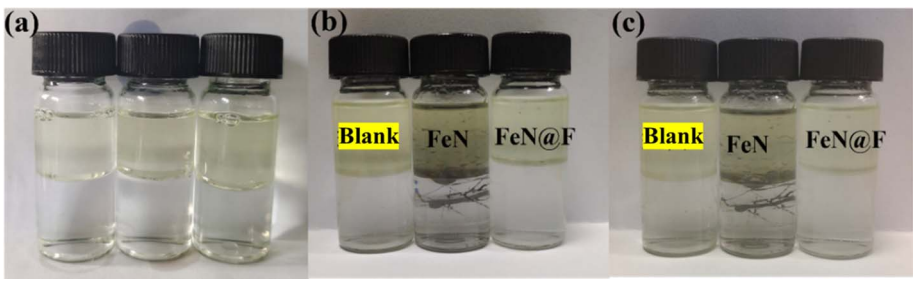

Fig. 6 Interfacial activity of blank group, Fe3N, and Fe3N@F (a) before shaking; (b) after shaking and standing for 20 min; (c) after shaking and standing for 24 h.

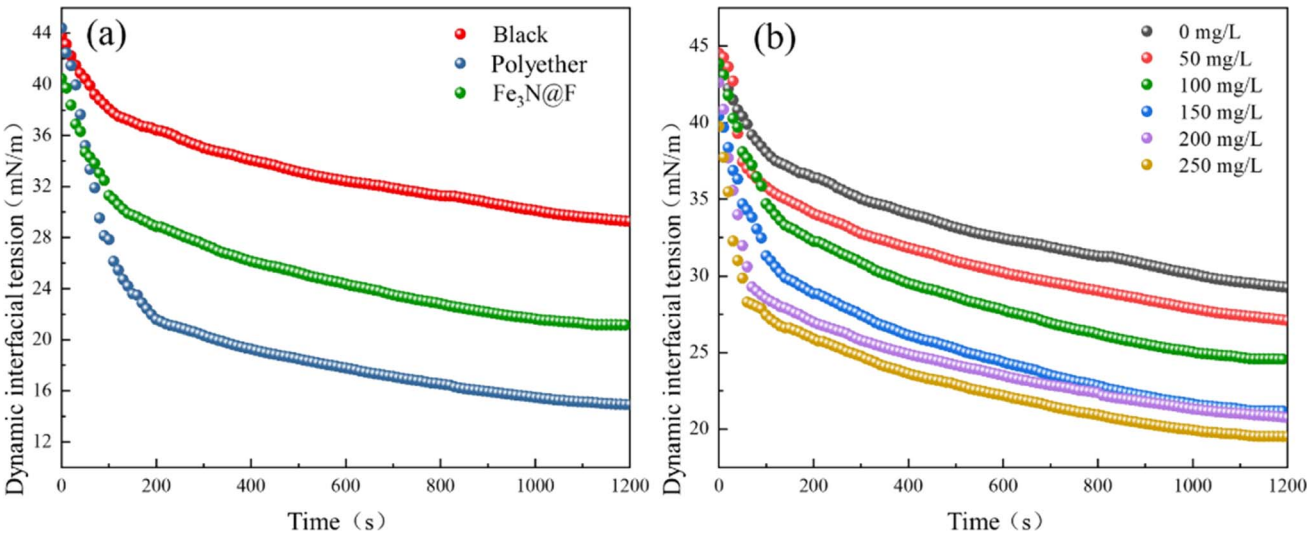

Fig. 7 Effect of different samples (a) and different dosages (b) of Fe_3N@F on interfacial tension.

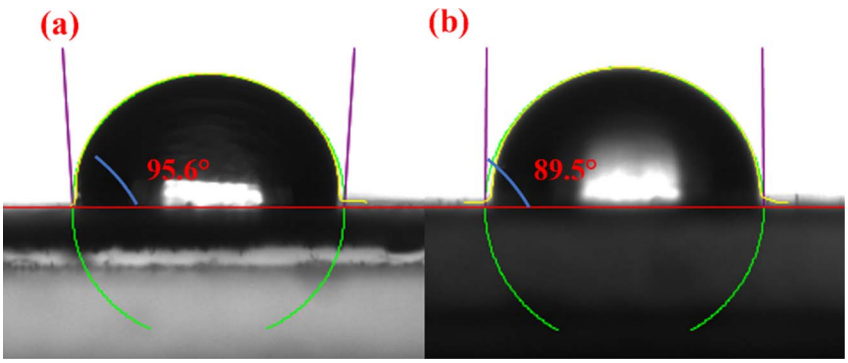

Fig. 8 Three-phase contact angles of (a) Fe_3N and (b) Fe_3N@F.

3.1.8 Magnetic property. Fig. 9 illustrates that the hysteresis loops of Fe_3N and Fe_3N@F demulsifier exhibit soft magnetic properties by passing through the origin. The saturation magnetization intensity (Ms) of Fe_3N is measured at 111.4 emu g^{-1}. Upon addition of varying mass ratios of fluorinated polyether, the saturation magnetization intensity of Fe_3N@F demulsifier decreased to different extents. With an increase in fluorinated polyether content, there was a greater reduction in the saturation magnetization intensity of Fe_3N@F demulsifier. This can be attributed to the higher content of fluorinated polyether causing more extensive wrapping around the Fe_3N particles, thereby impeding their magnetic properties and reducing their saturation magnetization intensity. Notably, no significant phase transformation was observed in Fe_3N.

3.2 The demulsifying performance of different magnetic demulsifiers

In order to further verify the demulsification performance of demulsifier, the characterization experiment of demulsification performance was carried out with heavy oil. Fig. 10 illustrates the impact of various materials on the demulsification of crude oil emulsion. The groups 1–6 correspond to the control, fluorinated polyether addition, Fe_3N@F1, Fe_3N@F2, Fe_3N@F3 and Fe_3N@F4 respectively. The untreated crude oil emulsion appears black with minimal demulsification effect; however, significant improvement is observed upon addition of fluorinated polyether. Furthermore, introduction of the Fe_3N@F series demulsifiers not only enhances the demulsification rate but also results in a clearer appearance of the crude oil emulsion. Comparative analysis reveals that the clearest emulsion is achieved after adding Fe_3N@F3. As successive additions are made from Fe_3N@F1 to Fe_3N@F3, clarity increases progressively; however turbidity sets in with the inclusion of Fe_3N@F4. Fig. 11 presents data on demulsification effects of different materials on crude oil emulsion. Following material addition, varying degrees of improvement in demulsification rates are observed. Notably, superior performance is demonstrated by Fe_3N@F3 with an impressive 89.2% demulsification rate. The effectiveness of the Fe_3N@F series surpasses that of individual fluorinated polyether monomers suggesting a synergistic effect during demulsification processes which enhances overall performance. The trend indicates an increase in demulsification rates from Fe_3N@F1 to Fe_3N@F3 while a decrease is noted

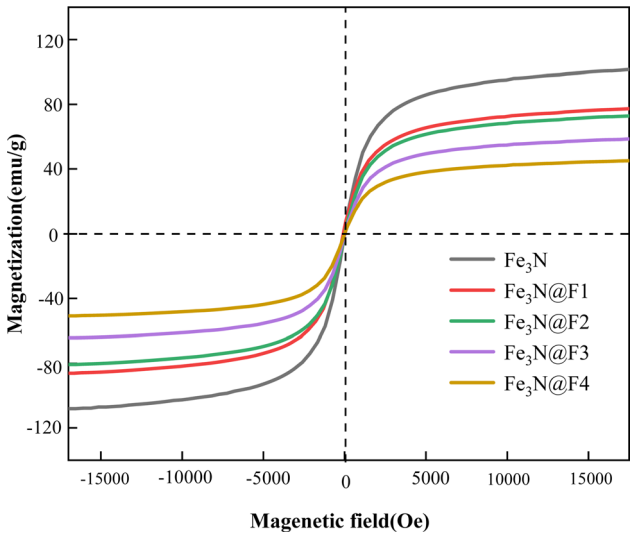

Fig. 9 Magnetization hysteresis loops of Fe_3N and Fe_3N@F demulsifier.

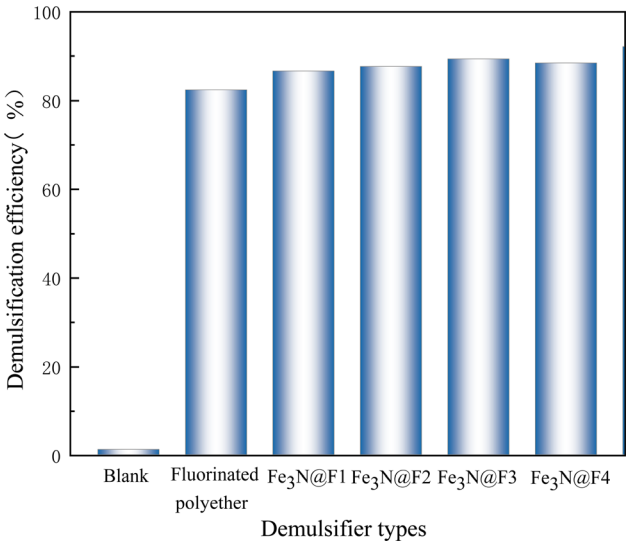

Fig. 11 Demulsification data for crude oil emulsions using different materials.

for Fe_3N@F4 consistent with observations depicted in Fig. 10. This may be attributed to uniform attachment when fluorinated polyether content is low whereas increased content leads to encapsulation and coverage over nitride iron thereby limiting its adsorption capacity and inhibiting synergistic action between both components. Comparison highlights superior emulsion inhibition effects achieved by Fe_3N@F3 as compared to other materials.

3.3 Effect of emulsifier dosage on demulsification performance

Following the aforementioned analysis, Fe_3N@F3 was determined to be the optimal demulsifier due to its exceptional demulsification effectiveness. Various quantities of Fe_3N@F3 were added to 20 mL of crude oil emulsion, and the demulsification process lasted for 150 minutes. The influence of demulsifier dosage on demulsification efficiency was examined, as illustrated in Fig. 12. This figure presents the demulsification rate of Fe_3N@F demulsifier ranging from 0 mg L^{-1} to 250 mg L^{-1}. The crude oil emulsion gradually became clearer while the demulsification rate consistently increased. However, there was only a slight increase of 0.1% in the demulsification rate between dosages of 150 mg L^{-1} and 200 mg L^{-1}, accompanied by heightened adhesion of crude oil to surfaces and increased turbidity within the emulsion. Analysis revealed that

Fig. 10 The demulsification effects of different materials on crude oil emulsions.

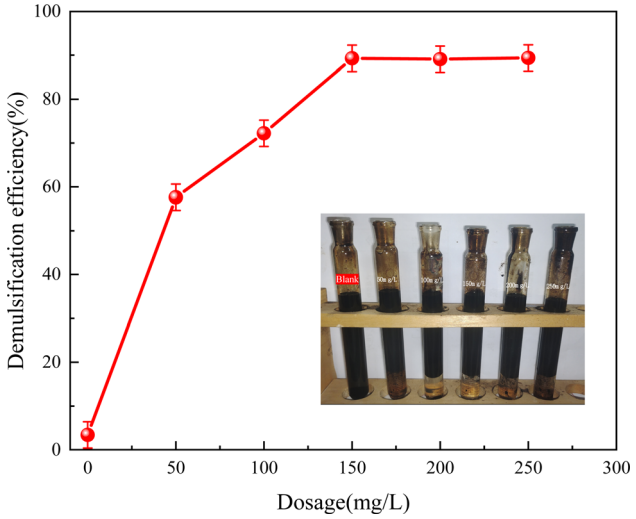

Fig. 12 Effects of the dosage of Fe_3N@F3 for the demulsification of crude oil emulsions.

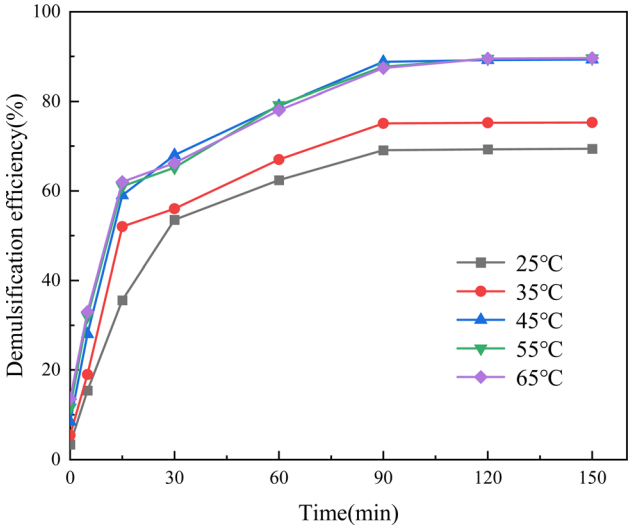

Fig. 13 Effects of the varying demulsification temperatures and sedimentation durations of Fe_3N@F3 for the demulsification of crude oil emulsions.

at a dosage level of 200 mg L^{-1}, the highest recorded demulsification rate reached an impressive 89.4%. This aligns with traditional usage principles for demulsifiers; as their dosage increases, more molecules are adsorbed at the oil–water interface displacing natural emulsifying agents on membranes and subsequently enhancing overall efficiency in breaking down emulsion structures.[28] However, once a certain concentration threshold is exceeded, saturation occurs regarding molecule adsorption at the oil–water interface leading to undesirable outcomes such as thickening surface films on dispersed phase liquid droplets or even formation of new interface films which can trigger unwanted occurrences like re-emulsification thereby diminishing overall effectiveness in separating phases.[29,30]

3.4 Effect of emulsification temperature and time on demulsification performance

The demulsification efficiency of Fe_3N@F3 demulsifier at an addition of 150 mg L^{-1} is depicted in Fig. 13 under various temperatures and durations. It is evident from the graph that with increasing temperature and time, the demulsification efficiency of Fe_3N@F3 steadily rises, reaching equilibrium around 90 minutes. Even after prolonged demulsification, the rate only experiences a marginal increase of less than 1%. Furthermore, the demulsification rate stabilizes at 45 °C, showing no significant variation as temperature continues to rise. This indicates that elevating the temperature can reduce the viscosity of oil-in-water emulsion and enhance molecular Brownian motion, thereby improving demulsification efficiency.[31,32] However, high temperatures may disrupt the rigid interface film of asphaltquinone in oil-in-water emulsion, making it easier for the demulsifier to be adsorbed and replaced, consequently enhancing oil–water separation effect. As a result, there is no substantial increase in demulsification efficiency at 55 °C. Therefore, setting a reaction time of 90 minutes and a demulsification temperature of 45 °C is recommended.

3.5 Regeneration and reusability of Fe_3N@F

Fig. 14 illustrates the emulsification inhibition performance of Fe_3N@F magnetic demulsifier after seven times recycled. The demulsification efficiency of Fe_3N@F decreases with an increasing number of recycling cycles, as evidenced by the decrease in demulsification rate from 89.4% to 68.2% following 7 cycles of reutilization, demonstrating outstanding demulsification performance of the Fe_3N@F. This decline is primarily attributed to the gradual accumulation of asphaltenes and resins within the crude oil emulsion on the demulsifier's surface, impeding its adsorption capacity. Consequently, the synthesized Fe_3N@F magnetic demulsifier exhibits commendable performance in inhibiting emulsification and can be recycled multiple times, resulting in economic benefits.

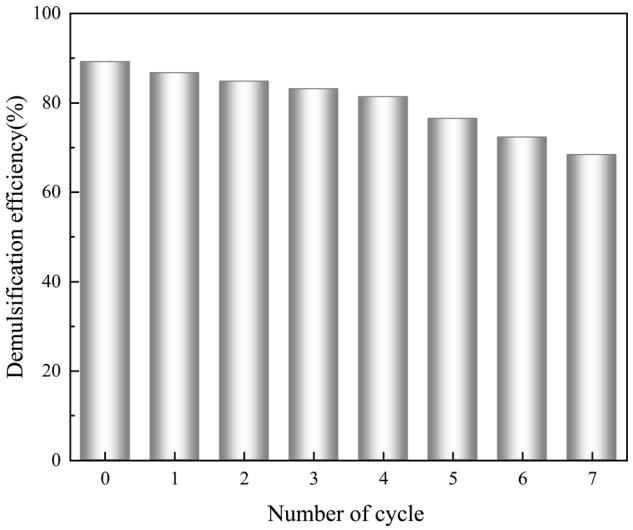

Fig. 14 The demulsification efficiency of Fe_3N@F at various cycling intervals.

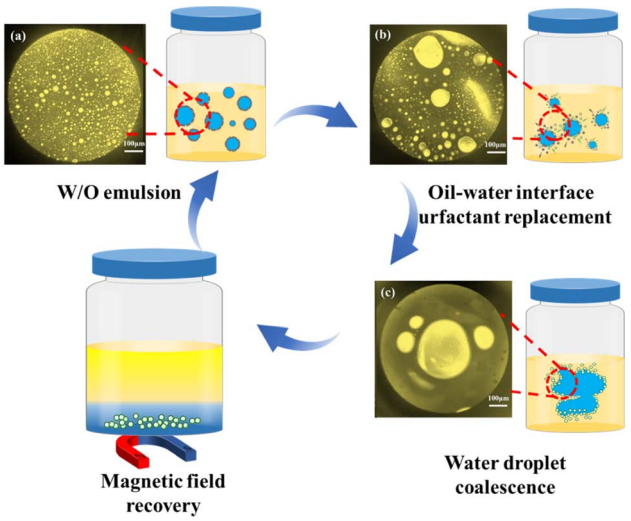

Fig. 15 The demulsification mechanism of crude oil emulsion, including microscopic images before (a), during (b), and after (c) demulsification.

3.6 Demulsification mechanism

The demulsification mechanism of the Fe_3N@F magnetic emulsifier is depicted in Fig. 15. To investigate the demulsification mechanism of Fe_3N@F magnetic emulsion breaker-driven crude oil emulsion, the microscopic state of the droplets within the crude oil emulsion before and after demulsification was observed using polarized light microscopy. From Fig. 15(b), the original crude oil emulsion exhibits uniform dispersion of fine water droplets, indicating a relatively stable emulsion system. By introducing Fe_3N@F magnetic demulsifier the natural surface-active substances at the oil–water interface were displaced and the interfacial membrane was disrupted, which led to the coalescence of tiny droplets within the crude oil emulsion, resulting in larger droplets with a reduced overall number, as illustrated in Fig. 15(b).[33,34] Fig. 15(c) depicts the microstructural characteristics of the emulsion during the demulsification phase, wherein a distinct oil–water interface is observed, indicating effective separation of oil and water. The aforementioned findings suggest that the Fe_3N@F magnetic demulsifier exhibits favorable coalescence, flocculation, and bridging capabilities.

4. Conclusion

This paper employed a one-pot synthesis method to fabricate four variations of Fe_3N@F magnetic demulsifiers using different ratios of nitrided iron and fluorinated polyether as the primary materials. All demulsifiers exhibited soft magnetic properties, with the saturation magnetization intensity of Fe_3N@F demulsifier decreasing as the proportion of fluorinated polyether increased. The experimental findings indicate that the Fe_3N@F3 demulsifier, produced through a 1 : 7 combination of Fe_3N and fluorinated polyether, exhibits the most effective demulsification properties. At a demulsifier dosage of 150 mg L^{-1} and a demulsification temperature of 45 °C, the highest demulsification rate reaches 89.4% after a 90 minutes treatment period. Furthermore, even after six cycles of use, it continues to demonstrate significant demulsification effectiveness. The outstanding interfacial activity, dynamic interfacial tension, and wetting properties of Fe_3N@F indicate its favorable hydrophilic–lipophilic balance, which confers upon it an extremely efficient demulsification ability and facilitates rapid migration to the oil–water interface, thereby promoting the coalescence of dispersed phase droplets. The utilization of iron nitride in demulsification surpasses the magnetic constraints imposed on demulsifiers by Fe_3O_4, offering a fresh approach for the advancement of magnetic demulsifiers.

Data availability

All relevant data are within the manuscript and its additional files.

Conflicts of interest

There are no conflicts to declare.

Acknowledgements

This study was funded by the Natural Science Foundation of Heilongjiang province, China (LH2022E025). This study was funded by the guiding Science and Technology Planning Projects of Daqing City (zd-2023-14). This study was funded by Basic research expenses for undergraduate universities in Heilongjiang Province (wg20240814).

References

1 D. Wang, D. Yang, C. Huang, Y. Huang and H. Zeng, Stabilization mechanism and chemical demulsification of water-in-oil and oil-in-water emulsions in petroleum industry: A review, *Fuel*, 2021, **286**(3), 119390.
2 H. Zhao, W. Kang, H. Yang, Z. Huang and B. Sarsenbekuly, Emulsification and stabilization mechanism of crude oil emulsion by surfactant synergistic amphiphilic polymer system, *Colloids Surf., A*, 2021, **609**(1–2), 125726.
3 O. R. Alara, N. H. Abdurahman, M. O. Tade, H. A. Ali and K. T. Alao, Demulsifier: An Important Agent in Breaking Crude Oil Emulsions, *Chem. Eng. Technol.*, 2022, (10), 45.
4 S. Faizullayev, A. Adilbekova, W. Kujawski and M. Mirzaeian, Recent demulsification methods of crude oil emulsions – Brief review, *J. Pet. Sci. Eng.*, 2022, 125726.
5 M. A. Saad, M. Kamil, N. H. Abdurahman, R. M. Yunus and O. I. Awad, An Overview of Recent Advances in State-of-the-Art Techniques in the Demulsification of Crude Oil Emulsions, *Processes*, 2019, **7**(7), 470.
6 H. Sun, X. Li, D. Liu and X. Li, Synergetic adsorption of asphaltenes and oil displacement surfactants on the oil-water interface: Insights on stabilization mechanism of the interfacial film, *Chem. Eng. Sci.*, 2021, **245**, 116850.
7 F. Xiao-Jun, T. Yin-Jun, Y. Yin, W. Gang, M. Ping and L. Lu, Relationship between the dynamic interfacial activity and

demulsification performance of hyperbranched poly(amido amine) polyethers, *Colloids Surf., A*, 2022, **633**(P2), 127869.

8 Y. Ning, Y. Kai-Yao, M. Ping and L. Lu, Dynamic interfacial activity and dilational viscoelasticity of polyether demulsifiers at the oil/water interface, *J. Mol. Liq.*, 2022, **363**, 119875.

9 Z. Jian, W. Xiujun, L. Qiang, D. Ming, F. Shenwen, Z. Chunsheng, *et al.*, Demulsification law of polyether demulsifier for W/O crude oil emulsion containing hydrophobically modified polyacrylamide in water, *J. Mol. Liq.*, 2024, **394**, 123805.

10 Z. Jingjing, Z. Xincheng, H. Lin, S. Hong and L. Xingang, Nano-modification of carboxylated polyether for enhanced room temperature demulsification of oil-water emulsions: Synthesis, performance and mechanisms, *J. Hazard. Mater.*, 2022, **439**, 129654.

11 Y. Zhang, H. Liu and G. Xia, Synthesis and Research of Highly Efficient Polyether Demulsifier, *ChemistrySelect*, 2022, (25), 7.

12 R. Zhou, Y. Jin, Y. Shen, S. Lai and P. Zhao, Surface activity, salt and pH tolerance, and wettability of novel nonionic fluorinated surfactants with a short fluorocarbon chain, *J. Dispersion Sci. Technol.*, 2020, 1–8.

13 H. S. M. Shakil, A. A. Adewunmi, M. Ahmad, M. Mobeen, Z. Xianmin and K. M. Shahzad, Fluorinated surfactants: A review on recent progress on synthesis and oilfield applications, *Adv. Colloid Interface Sci.*, 2022, **303**, 102634.

14 L. Wei, L. Zhang, S. Guo, X. Jia, Y. Zhang, C. Sun, *et al.*, Synthesis and Study of a New Type of Fluorinated Polyether Demulsifier for Heavy Oil Emulsion Demulsification, *ACS Omega*, 2021, **6**(39), 25518–25528.

15 L. Zhang, L. Wei, L. Shi, X. Dai, S. Guo, X. Jia, *et al.*, Synthesis and characterization of a novel reticulated multi-branched fluorinated polyether demulsifier for w/o emulsion demulsification, *J. Polym. Res.*, 2022, **29**(5), 164.

16 G. Xiaoheng, L. Changjun, Z. Lin, G. Haiying, S. Changqing, J. Xinlei, *et al.*, Screening and Demulsification Mechanism of Fluorinated Demulsifier Based on Molecular Dynamics Simulation, *Molecules*, 2022, **27**(6), 1799.

17 X. Zhang, T. Lu and J. Huang, Demulsification of surfactant-rich emulsion systems by using amphiphilic or positively charged magnetic nanoparticles, *Sep. Purif. Technol.*, 2024, **347**, 127587.

18 A. A. Adewunmi, M. S. Kamal and T. I. Solling, Application of magnetic nanoparticles in demulsification: A review on synthesis, performance, recyclability, and challenges, *J. Pet. Sci. Eng.*, 2020, **196**, 107680.

19 C. Liu, L. Wei, W. Qin, Y. Gu and X. Jia, Fluorinated polyether-coated Fe_3O_4-functionalized oxidized carbon nanotubes as a recyclable demulsifier for crude oil emulsion treatment, *RSC Adv.*, 2024, **14**(5), 2862–2872.

20 X. J. Feng, X. He, L. Lai, Q. Lu and J. Wu, Polydopamine-anchored Polyether on Fe_3O_4 as Magnetic Recyclable Nanoparticle-Demulsifiers, *Colloids Surf., A*, 2021, **617**, 126142.

21 S. Hamed, M. Zahra and A. Ebrahim, Nanomagnetic Cyclodextrin decorated with ionic liquid as green and reversible Demulsifier for breaking of crude oil emulsions, *Carbohydr. Polym.*, 2024, **327**, 121697.

22 N. Zhao, W. Wang, L. Xiang, Z. Ye, X. Chen, H. Ding, *et al.*, Synthesis, structure and magnetic properties of Fe_3N nanoparticles, *J. Mater. Sci.: Mater. Electron.*, 2017, 15701–15707.

23 T. He, M. Tu, J. Zhang, *et al.*, Nanoparticles of iron nitride encapsulated in nitrogen-doped carbon bulk derived from polyaniline/Fe_2O_3 blends and its electrochemical performance, *Part. Part. Syst. Charact.*, 2020, **37**(7), 2000132.

24 Y. L. Tan, Zhi. Design, preparation and characterization of iron nitride magnetic abrasives, *J. Alloys Compd.*, 2019, **774**, 443–450.

25 H. Wang, Y. Wu, Z. Wu, Z. Liu, H. Yang and Y. Xie, Preparation of a low-temperature poly (amino acids) demulsifier and its demulsification mechanism, *Fuel*, 2024, **365**, 131237.

26 S. Jiang, Q. Li, B. Xu, T. Zou, Y. Zhang, W. Ping, *et al.*, Synthesis and Application of a Novel Multi-Branched Block Polyether Low-Temperature Demulsifier, *Molecules*, 2023, **28**(24), 8109.

27 X. Xia, J. Ma, F. Liu, H. Cong and X. Li, A Novel Demulsifier with Strong Hydrogen Bonding for Effective Breaking of Water-in-Heavy Oil Emulsions, *Int. J. Mol. Sci.*, 2023, **24**(19), 14805.

28 J. Xinlei, W. Lixin, F. Mingming, L. Chao, G. Yuxin, Q. Weining, *et al.*, One-pot preparation of environmentally friendly, high demulsification rate and novel functional magnetic demulsifier: Used for oil and water separation in crude oil emulsion, *Arabian J. Chem.*, 2023, **16**(10), 105134.

29 D. Wang, D. Yang, C. Huang, Y. Huang and H. Zeng, Stabilization mechanism and chemical demulsification of water-in-oil and oil-in-water emulsions in petroleum industry: A review, *Fuel*, 2021, **286**(3), 119390.

30 A. Miadonye and M. Amadu, Theoretical Interpretation of pH and Salinity Effect on Oil-in-Water Emulsion Stability Based on Interfacial Chemistry and Implications for Produced Water Demulsification, *Processes*, 2023, **11**(8), 2470.

31 W. Kang, X. Yin, H. Yang, *et al.*, Demulsification performance, behavior and mechanism of different demulsifiers on the light crude oil emulsions, *Colloids Surf., A*, 2018, **545**, 197–204.

32 Y. Gu, L. Wei, C. Liu, *et al.*, Fluorinated polyether grafted TiO_2 magnetic composite material for oil-water separation of crude oil emulsion, *J. Dispersion Sci. Technol.*, 2023, **45**, 1296–1306.

33 G. Zlata and T. Siwar, Mechanisms, performance optimization and new developments in demulsification processes for oil and gas applications, *Adv. Colloid Interface Sci.*, 2018, **260**, S0001868618301957.

34 F. Yang, P. Tchoukov, P. Qiao, *et al.*, Studying demulsification mechanisms of water-in-crude oil emulsions using a modified thin liquid film technique, *Colloids Surf., A*, 2018, 215–223.